

# GMRT observations of NGC 2997 and radio detection of the circumnuclear ring

J. Kodilkar,<sup>1\*</sup>, N. G. Kantharia,<sup>1</sup> S. Ananthkrishnan<sup>2</sup>

<sup>1</sup>National Centre for Radio Astrophysics, Tata Institute of Fundamental Research, Post Bag 3, Ganeshkhind,

<sup>2</sup>Dept. of Electronic Science, Pune University,  
Pune 411 007, India

Accepted 2011 May 12. Received 2010 Aug 09; in original form 2010 July 9

## ABSTRACT

We present high-resolution, high-sensitivity radio continuum observations of the nearby spiral galaxy NGC 2997 at 332, 616 and 1272 MHz using the Giant Metrewave Radio Telescope (GMRT). The integrated spectrum of this galaxy has a spectral index of  $-0.92$  ( $S_\nu \propto \nu^\alpha$ ) and we place an upper limit to the thermal fraction at 1272 MHz of  $\sim 10$  per cent. Our multi-frequency study shows a relatively flat spectrum source ( $\alpha \sim -0.6$ ) at the centre of the galaxy. This leads to radio detection of a circumnuclear ring in the high resolution map at 1272 MHz. We detect five hotspots in the ring, with average star formation rate of  $\sim 0.024 M_\odot \text{ yr}^{-1}$ , a median SN rate of  $\sim 0.001 \text{ yr}^{-1}$  and luminosity of  $10^{20} \text{ W Hz}^{-1}$ . We estimate an equipartition field in the central nuclear region of diameter  $\sim 750 \text{ pc}$  to be about  $30 \mu\text{G}$ . We also report several interesting features along the spiral arms. In this paper, we present the low frequency radio continuum maps, the spectral index distribution, the circumnuclear ring and the derived physical properties.

**Key words:** galaxies: individual: NGC 2997- radio continuum: galaxies - galaxies: nuclei - galaxies: statistics

## 1 INTRODUCTION

NGC 2997 is an interesting grand design spiral galaxy of type SAB(rs)c located in the loose galaxy group LGG 180 (Garcia 1993). The disc inclination is  $\sim 40^\circ$  (Milliard & Marcelin 1981) and the southern part of the disc is closer to us (Peterson 1978). We assume a distance of 13.8 Mpc (Tully 1988) to NGC 2997 and note that 1 arc-min corresponds to a linear scale of  $\sim 4.0 \text{ kpc}$ . Basic data on NGC 2997 are listed in Table 1.

The photometric and morphological analysis of this galaxy shows the presence of a normal nucleus surrounded by several HII regions known as ‘hotspots’ (Pastoriza 1975). Further investigations in optical (Meaburn & Terrett 1982), ultraviolet (Maoz et al. 1996) and near-infrared (Elmegreen et al. 1999) have detected a circumnuclear star-forming ring in NGC 2997. The study of such a ring is significant in terms of understanding gas transport to the inner regions of the galaxy and its association with any possible nuclear activity. NGC 2997 also shows several bright knots of emission along its arms. These knots are young star clusters with typical masses of  $\sim 5 \times 10^4 M_\odot$  (Grosbøl et al. 2006). This galaxy also hosts two giant HII regions which show supersonic velocity dispersion caused by an intense starburst (Firpo et al. 2005). The galaxy which is part of the HI brightest galaxy catalogue of the southern

sky derived from HIPASS has an HI mass of  $\sim 4.2 \times 10^9 M_\odot$  and half power line width of  $254 \text{ km s}^{-1}$  (Koribalski et al. 2004).

NGC 2997 has been extensively studied in radio wavelengths shorter than 20 cm by Han et al. (1999) and Men & Han (2005). To the best of our knowledge, this galaxy has not been studied at longer wavelengths ( $\lambda > 20 \text{ cm}$ ). Since the non-thermal spectrum of synchrotron radiation is dominant at low frequencies, the GMRT observations at metre-wavelengths with high angular resolution and high sensitivity can reveal many significant features of NGC 2997 due to its moderate inclination such as smooth synchrotron emission from the disc, morphological structure of spiral arms, nucleus and compact HII regions. The spectral index distribution study of NGC 2997 could be useful for identification of giant HII regions.

The low radio frequency spectrum of the galaxy is important in obtaining the non-thermal spectral index of the galaxy which can then be used to separate the thermal and non-thermal contributions to the observed spectrum. Moreover, the non-thermal luminosities at low frequencies can be used to estimate the supernovae rate ( $\text{yr}^{-1}$ ), average star formation rate ( $M_\odot \text{ yr}^{-1}$ ), production rate of the Lyman continuum photons ( $\text{s}^{-1}$ ) etc for the galaxy.

In this paper, we present radio continuum observation of NGC 2997 using the GMRT (Ananthkrishnan 2005; Swarup et al. 1991) at 332, 616 and 1272 MHz. Section 2 describes the observations and the data reduction procedure. Section 3 presents the total intensity maps and the morphological details of radio continuum features of NGC 2997. In section 4, we discuss the total emission

\* Email: jitendra@ncra.tifr.res.in (JK); nimisha@ncra.tifr.res.in (NGK); subra.anan@gmail.com (SAK)

**Table 1.** Basic data on NGC 2997<sup>†</sup>

Optical center (J2000)	09h45m38.8s -31d11'28''
Morphological type <sup>‡</sup>	SAB(rs)c
Major diameter (arcmin)	8.9
Minor diameter (arcmin)	6.8
Distance ( $H_0 = 75 \text{ km s}^{-1} \text{ Mpc}^{-1}$ )	13.8 Mpc
Magnitude (Visual)	10.06
Inclination angle (deg.)	40
Heliocentric radial velocity ( $\text{km s}^{-1}$ )	$1088 \pm 2$

<sup>†</sup>Reference : NASA/IPAC Extragalactic Database (NED)

<sup>‡</sup>de Vaucouleurs et al. (1991)

spectrum of the galaxy, the spectral index map derived between 1272 and 332 MHz and the circumnuclear ring. The last section summarizes the paper.

## 2 OBSERVATIONS AND DATA REDUCTION

We had a total of three observing sessions on NGC 2997 using the GMRT synthesis array at each of the three frequency bands 332, 616 and 1272 MHz respectively. Observing sessions were conducted in the period from 2003 to 2004 using the standard spectral line mode of the GMRT digital correlator which gives visibility data of 16 MHz bandwidth across 128 channels for two polarisations. The observational parameters are summarized in Table 2. The raw visibility data were converted to FITS and analysed using standard AIPS<sup>1</sup>.

The VLA flux density calibrators, 3C147 and 3C286 were used as flux density reference to scale the flux densities of phase calibrators and the target source. To correct the ionospheric and instrumental gain variations, phase calibrator 0837-198 was observed for 6 min during every 25 min of observation of the target source. The flux density values of phase calibrators obtained using the task GETJY are given in Table 2. The flux density calibrators were also used for bandpass calibration. To avoid bandwidth smearing effect, the band-pass calibrated data at 616 and 1272 MHz band were collapsed to five channels each of  $\sim 2.75$  MHz bandwidth by averaging every 22 channels. At 332 MHz, ten channels each of  $\sim 1.25$  MHz bandwidth formed from RFI free band by averaging every 10 channels. The expected error bars in flux density scale for the GMRT observations are  $\lesssim 10$  per cent.

First, a low resolution map of  $\sim 45$  arcsec was made using 'uvtaper' at each observing frequency and the entire primary beam was imaged. We also used varying tapers to generate maps of different angular resolution which can be compared at the different frequencies. There were two to three strong point sources near the edge of primary beam at each frequency with peak flux ten to twelve times stronger than the peak flux on the object. These sources were removed using the task UVSUB.

Wide field imaging was used at 616 and 332 MHz. The number of facets used for imaging NGC 2997 at 616 and 332 MHz were 13 and 22 respectively (obtained using SETFC task in AIPS). No self calibration was done at 1272 MHz. At other frequencies, the visibility data sets were first phase self-calibrated using only strong point sources near or within the inner quarter of the primary

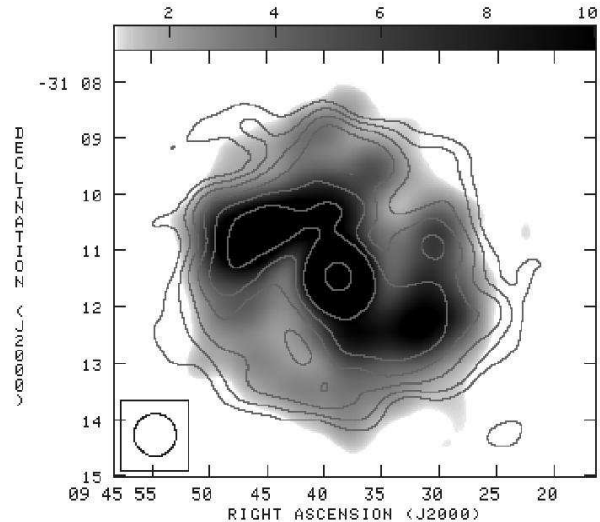


**Figure 2.** shows the GMRT 1272 MHz radio contour map of NGC 2997 with a beamsize of 45 arcsec overlaid on the NVSS 1400 MHz grey scale image (Condon et al. 1998). The disc extent and morphology of the GMRT low resolution map is similar to the NVSS image indicating that the GMRT map is sensitive to large scales. The rms  $\sigma$  is 0.6 mJy per beam area, contours starting from  $3\sigma$  level and scaled by factor  $\sqrt{2}$ .

field. After two to three iterations of phase self-calibration using only point sources, the source model obtained by cleaning up to the rms noise level of the map was included in self-calibration. At 332 and 616 MHz, it took about four to six iterations to get good convergence of self-calibration resulting in improved dynamic range maps. All facets were combined and primary beam correction applied using the FLATN task to produce a map at each observing frequency.

## 3 OBSERVATIONAL RESULTS

### 3.1 Total intensity maps

We made total intensity maps of the object with angular resolution ranging from 45 to 3 arcsec. Whenever possible, the total intensity maps at different observing frequencies were made with a similar angular resolution by using the uv-tapering function in the task 'IMAGR'. Fig.1 shows the total intensity maps of NGC 2997 at 1272, 616 and 332 MHz at a resolution of 15 arcsec overlaid on the optical Digitized Sky Survey image. The uv-tapering and weighting functions used while mapping the object are given in Table 3.

The multifrequency total intensity GMRT maps in Fig. 1 show about six common radio continuum features of NGC 2997. These discrete features are labelled by numbered tags in Fig.1a. In Table 4, we summarize their positions, size, observed flux densities, etc. The peak positions of the discrete features listed in Table 4 match within median errors of  $\Delta \text{RA} \sim \pm 0.22^s$  and  $\Delta \text{DEC} \sim \pm 2$  arcsec. The summary of radio continuum emission features seen in NGC 2997 is as follows :

(i) The radio disc in the GMRT low-resolution images has an extent of  $\sim 6.5'$  by  $8'$  which is comparable to the optical extent. The extent of radio emission in the low resolution map at 1272 MHz is comparable to the NVSS grey-scale image (Condon et al. 1998) as shown in Fig.2.

<sup>1</sup> Astronomical Image Processing System, distributed by the National Radio Astronomy Observatory, <http://www.aips.nrao.edu>. The NRAO is a facility of the National Science Foundation operated under cooperative agreement by Associated Universities, Inc.

Figure 1. The total intensity maps of NGC 2997 with a resolution of 15 arcsec at 1272, 616, and 332 MHz.

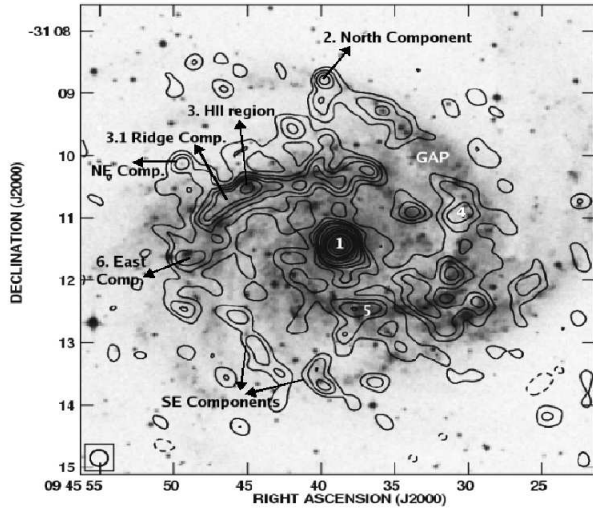


Fig. 1a : The 1272 MHz radio contour map superimposed on the optical Digitized Sky Survey image. The six discrete radio continuum features detected at three wavebands are labelled with numbers. The peak brightness is  $21 \text{ mJy beam}^{-1}$ . The rms  $\sigma$  is  $0.3 \text{ mJy}$  per beam area, the beam is depicted at the bottom left corner. The contours are at  $(-3, 3, 5, 7, 9, 11, 15, 20, 25, 30, 40, 50, 60, 70) \times \sigma$

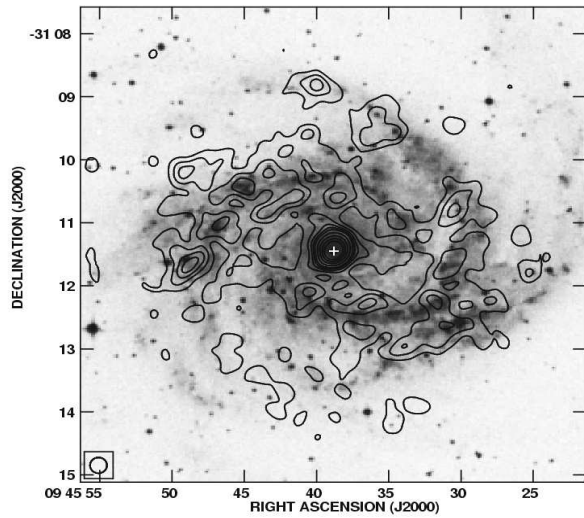


Fig. 1b : The 616 MHz radio contour map overlaid on the DSS optical image. The radio peak position of the nucleus is marked as a plus sign. The peak brightness is  $28.4 \text{ mJy beam}^{-1}$ . The rms  $\sigma$  is  $0.6 \text{ mJy}$  per beam area, the beam size is depicted at the bottom left corner. Contours :  $(-3, 3, 5, 7, 9, 11, 15, 20, 25, 30, 40) \times \sigma$

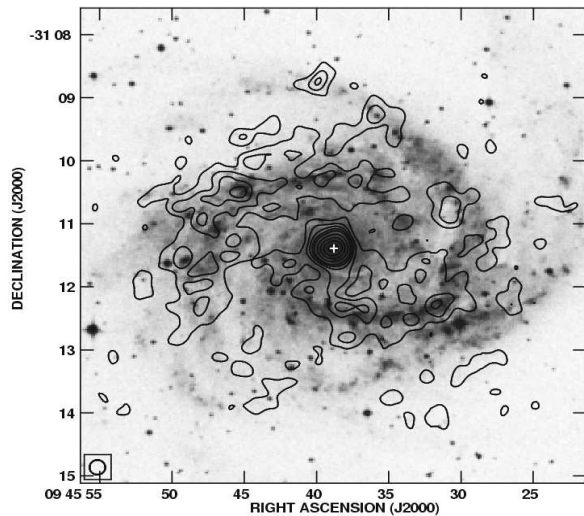


Fig. 1c : The 332 MHz radio contour map overlaid on the DSS optical image. The radio peak position of the nucleus is marked as a plus sign. The peak brightness is  $40.9 \text{ mJy beam}^{-1}$ . The rms  $\sigma$  is  $1 \text{ mJy}$  per beam area, the beam size is shown at the BLC. Contours :  $(-3, 3, 5, 7, 9, 11, 15, 20, 25, 30, 40) \times \sigma$ .

**Table 2.** Observation table

Observing band (MHz)	332	616	1272
1. Date	2004 Feb 24	2003 Jan 21	2003 Aug 16
2. Correlator used (USB/LSB) <sup>a</sup>	USB	USB	LSB
3. On source time(Hrs.) <sup>b</sup>	5	4	3
4. Receiver bandwidth (MHz)	16	16	16
5. No. of working antennas <sup>c</sup>	27	24	28
6. Shortest spacing(k $\lambda$ )	0.06	0.120	0.250
	$\sim 55$ m	$\sim 60$ m	$\sim 58$ m
7. Longest spacing(k $\lambda$ )	27	40	101
	$\sim 25$ km	$\sim 20$ km	$\sim 24$ km
8. Largest visible structure <sup>d</sup>	$\sim 19'$	$\sim 12'$	$\sim 8'$
9. Flux density calibrator(s)	3C147,3C286	3C147,3C286	3C147,3C286
Flux density in Jy <sup>e</sup>	52.69,25.96	38.26,21.07	23.69,15.48
10. Phase calibrator(s)	0837-198,0902-142	0837-198	0837-198
Flux density in Jy <sup>f</sup>	13.3 $\pm$ 0.4, 4.3 $\pm$ 0.1	8.7 $\pm$ 0.08	4.6 $\pm$ 0.1

a. USB-Upper side band, LSB-Lower side band. b. Total observation time on the object before editing. c. Maximum number of antenna operational at any time during the observation. d. Corresponding to the shortest spacing present in our data. e. Set by SETJY task : Using VLA (1999.2) or Reynolds (1934-638) coefficients. f. Flux density and error from GETJY.

**Table 3.** Map parameters

Figure	1a	1b	1c
Band Center (MHz) <sup>†</sup>	<b>1272</b>	<b>616</b>	<b>332</b>
Synthesized Beam <sup>a</sup>	15.8'' $\times$ 12.4'' @25°	17.9'' $\times$ 11.7'' @41°	15.9'' $\times$ 12.0'' @14°
Restoring Beam <sup>b</sup>	15''	15''	15''
UV-taper/Weighting	20 k $\lambda$ /NA	20 k $\lambda$ /NA	16 k $\lambda$ /UN
RMS noise (mJy beam <sup>-1</sup> )	0.3	0.6	1.0
Figure	2	5-contour	5-left grey <sup>c</sup>
Band Center (GHz) <sup>†</sup>	<b>1.27</b>	<b>1.27</b>	<b>4.8</b>
Synthesized Beam <sup>a</sup>	50.9'' $\times$ 36'' @11°	4.06'' $\times$ 2'' @11°	1.5'' $\times$ 0.7'' @55°
Restoring Beam <sup>b</sup>	45''	3''	3''
UV-taper/Weighting	5 k $\lambda$ /NA	None/UN	None/UN
RMS noise (mJy beam <sup>-1</sup> )	0.6	0.08	0.04

<sup>†</sup>All maps are stoke I and corrected for the shape of the GMRT primary beam.

NA-Natural weighting, UN-Uniform weighting.

Final bandwidth for analysis after editing is about  $\sim 12.5$  MHz at each frequency.

a. Synthesized beam for a deconvolution, position angle with respect to the major axis is given in degree.

b. Restoring beam is a circular Gaussian with PA=0 degree, and the area is approximated to the deconvolving beam area in square arcsec  $\Omega_s = 1.13 * \beta_{maj} \times \beta_{min}$ .

c. Map using the VLA archival data.

(ii) All our total intensity maps show the compact bright nucleus, centred at, RA=  $09^h 45^m 38.76^s$ ; DEC=  $-31^\circ 11' 26.60''$  (J2000). The uncertainties in RA and DEC are  $\sim 0.03^s$  and  $\sim 0.4$  arcsec, respectively. The radio peak position coincides with the values given by Han et al. (1999), Men & Han (2005) and also the optical centre (see Table 1). At first glance, the intense unresolved nucleus at 15 arcsec resolution (Fig.1) appears like an AGN.

(iii) The radio continuum emission associated with both the spiral arms is clearly detected in all the maps shown in Fig.1. There is an intense ridge of emission along the northern spiral arm as compared to the southern arm.

(iv) No radio emission is detected in the northern part of the southern spiral arm near the region at RA= $9^h 45^m 32.8^s$ ; DEC=  $-31^\circ 10'$  (labelled as 'GAP' in Fig. 1a). This region is bluer in the optical image, suggesting a young star forming complex. This gap has also been noted in the VLA total intensity maps at  $\lambda 20$ , 18, 6 cm and in the polarized intensity maps at  $\lambda 6$  and 13 cm (Han et al. 1999; Men & Han 2005).

(v) A bright compact source (component 2) is seen in all our maps of NGC 2997 at RA=  $09^h 45^m 39.6^s$ ; DEC=  $-31^\circ 08' 51.1''$ , in the north of the galaxy. No discrete optical counterpart is seen for this source.

(vi) All the maps in Fig.1 show an intense region (component 3) in the northern spiral arm, near RA=  $09^h 45^m 45^s$ ; DEC=  $-31^\circ 10' 33''$ . This compact region is coincident with the giant HII region identified by Firpo et al. (2005) using high resolution optical spectra ( $\lambda 3726 - 7136 \text{ \AA}$ ). Apart from this, a prominent north-east discrete component (labelled as 'NE Comp.') is seen in Figs. 1a and 1b, positioned at RA= $09^h 45^m 49.28^s$ , DEC=  $-31^\circ 10' 11.02''$  (J2000) and lying roughly above the northern ridge. This component appears to be a flat spectrum source since it is barely detected in the 332 MHz map (Fig. 1c).

#### Global radio continuum properties :

The integrated flux densities given in Table 5 are obtained by integrating the region above  $3\sigma$  contour in the low resolution maps (45 arcsec). The measured spectral power ranges from  $\sim 7.9 \times$

**Table 4.** Some discrete components in the disc of NGC 2997

Source	Observed position at 1272 MHz	Integrated flux densities (mJy) & Peak intensities (mJy beam <sup>-1</sup> ) at			Spectral index 332-1272 MHz	Comments
	$\alpha_{2000} = \text{h m s} \pm \text{s}$ $\delta_{2000} = \text{° ' ''} \pm \text{''}$	1272 MHz	616 MHz	332 MHz	( $S_\nu \propto \nu^\alpha$ )	
1	09 45 38.76 ± 0.0	38.7 ± 1.6	56.6 ± 3.1	86.3 ± 4.0	-0.6	Nuclear region
	-31 11 26.60 ± 0.3	21.0 ± 0.5	28.4 ± 1.2	40.9 ± 1.3	-0.5	
2	09 45 39.65 ± 0.1	13.7 ± 2.4	20.9 ± 4.8	21.0 ± 4.6	-0.31	North source
	-31 08 51.15 ± 2.1	4.2 ± 0.6	6.9 ± 1.2	8.1 ± 1.3	-0.48	
3	09 45 45.05 ± 0.1	16.7 ± 2.1	14.0 ± 4.6	12.04 ± 3.6	0.24	HII region in northern arm
	-31 10 33.08 ± 1.1	6.0 ± 0.6	4.9 ± 1.2	6.5 ± 1.4	-0.06	
3.1	09 45 45.87 ± 0.3	19.3 ± 3.7	27.0 ± 5.2	59.8 ± 14	-0.84	Northern ridge component (~5.0 kpc by 2.1 kpc)
	-31 10 41.19 ± 2.3	6.3 ± 0.5	6.8 ± 0.9	15.2 ± 1.2		
4	09 45 30.53 ± 0.2	5.3 ± 2.0	18.3 ± 5.6	22.6 ± 4.9	-1.08	Nonthermal north-west component
	-31 10 54.90 ± 4.1	2.1 ± 0.6	5.0 ± 1.2	8.0 ± 1.3	-0.98	
5	09 45 37.42 ± 0.3	6.1 ± 2.1	5.8 ± 3.2	15.6 ± 5.0	-0.69	Component in southern arm
	-31 12 28.48 ± 2.3	2.25 ± 0.5	3.42 ± 1.3	5.4 ± 1.3	-0.65	
6	09 45 48.84 ± 0.2	26.1 ± 4.4	13.3 ± 4.1	22.5 ± 5.3	0.11	East component of North-east arm
	-31 11 36.10 ± 2.5	3.9 ± 0.5	5.4 ± 1.2	7.3 ± 1.3	-0.45	

**Table 5.** Global radio continuum properties of NGC 2997

Observing band (MHz) →	332	616	1272
Flux density (mJy) †	1134 ± 111	730 ± 22	367 ± 8
Spectral Power (10 <sup>21</sup> W Hz <sup>-1</sup> )	24.4 ± 1.7	15.7 ± 0.3	7.9 ± 0.1
Global Spectral Index ( $S_\nu \propto \nu^\alpha$ )	332 → 616 : -0.71	616 → 1272 : -0.94	332 → 1272 : -0.84

†The reasonable error bars in flux density scale are expected to be  $\lesssim 10$  per cent.

$10^{21}$  W Hz<sup>-1</sup> at 1272 MHz to  $24.4 \times 10^{21}$  W Hz<sup>-1</sup> at 332 MHz. At 1.4 GHz, normal galaxies range in power from  $L \lesssim 10^{18}$  to  $\sim 10^{23}$  h<sup>-2</sup> W Hz<sup>-1</sup> where  $h \equiv H_0 / (100 \text{ km s}^{-1} \text{ Mpc}^{-1})$  (Condon 1992). The global spectral index values given in Table 5 indicate that the spectrum flattens at the lower frequencies. The total emission spectrum of many normal spiral galaxies with moderate surface brightness are known to show a break in the range from 0.1 to 1 GHz. One of the reasons for this is possibly free-free absorption by the cool ( $T_e < 1000$  K) ionized gas filling a large fraction of the radio emitting volume (Israel & Mahoney 1990). On the other hand, the break could be due to propagation effects of relativistic electrons and subsequent energy losses (Hummel 1991; Pohl, Schlickeiser, Hummel 1991)

The radio-selected samples of normal galaxies are characterized by the FIR/radio flux density ratios (Condon 1992). Helou et al. (1985) defined the parameter  $q$  as a logarithmic measure of the FIR/radio flux density ratio. For more general comparisons, the  $\hat{q}_{\text{FIR}}$  is defined as  $\hat{q}_{\text{FIR}} = \log\{S_\nu(\text{FIR})/[S_\nu(\text{rad}) \times (\nu_{\text{rad}}/1.4 \text{ GHz})^{-\alpha}]\}$  (Fitt et al. 1996), where  $\alpha$  is the radio spectral index ( $S_\nu \propto \nu^\alpha$ ). The spectral index for the observed GMRT data is  $-0.79 \pm 0.07$ . From the *IRAS* surveys (Fitt et al. 1996) at 60 and 100  $\mu\text{m}$  the flux densities of NGC 2997 are 32.28 and 85.14 Jy, respectively. Using the *IRAS* FIR flux density measurements and integrated flux densities measured with the GMRT, the derived  $\hat{q}_{\text{FIR}}$  parameter is  $\sim 2.19 \pm 0.03$ , which is close to the median for spiral galaxies at 1.4 GHz, i.e.  $\hat{q}_{\text{FIR}} \approx 2.30$  with the rms scatter  $\sigma_{\hat{q}} \lesssim 0.2$  (Condon & Broderick 1988; Condon et al. 1991b; Helou et al. 1985). The spectral power and FIR/radio flux density

ratio found at our observing frequencies confirms that NGC 2997 is a normal spiral galaxy.

## 4 DISCUSSION

### 4.1 The observed radio spectrum & SFR

Integrated flux densities of NGC 2997 obtained using the GMRT and other published data from 0.33 to 8.46 GHz are listed in Table 6. A single power law ( $S_\nu \propto \nu^\alpha$ ) with  $\alpha = -0.92 \pm 0.04$  gives the best-fitting to the radio spectrum from 0.33 to 5 GHz (Fig. 3). A value of  $\alpha = -1.10 \pm 0.07$  is quoted by Men & Han (2005) for the radio spectrum from 1.43 to 8.46 GHz. Niklas et al. (1997) analysed the radio continuum spectra of 74 galaxies to separate the thermal and the non-thermal radio emission. The mean value obtained for non-thermal spectral index is  $\langle \alpha_{nt} \rangle = -0.83 \pm 0.02$ . They also studied the correlation of the morphological type and non-thermal spectral index and found that spiral galaxies of type Sc show  $\alpha_{nt}$  to be in the range of  $-0.8$  to  $-1.05$ . Spectral index of NGC 2997 which is a Sc galaxy lies in the above range. The flatter spectrum  $\alpha = -0.79 \pm 0.07$  for the GMRT data at the lower frequencies compared to the wide band spectral index value could suggest a break in the spectrum at  $\nu < 1$  GHz. However the change in  $\alpha$  is only  $\sim 2\sigma$  and needs to be confirmed with data at still lower  $\nu$ .

Condon & Yin (1990) estimated a global thermal fraction for most of the normal galaxies, as  $S/S_{\text{th}} \sim 1 + 10 \left(\frac{\nu}{\text{GHz}}\right)^{(0.1 - |\alpha_{nt}|)}$ , where  $S$  is the total flux density, and  $S_{\text{th}}$  is the flux density due to the thermal component. Taking,  $\alpha_{nt} =$

−0.79, thermal fractions derived at 1272, 616 and 332 MHz are  $\sim 10$ , 6 and 4 per cent respectively of the measured total flux density value at each observing band. The derived thermal fraction at 1.2 GHz agrees with the obtained mean value of thermal fraction at 1 GHz for 74 galaxies by Niklas et al. (1997) which is  $\langle f_{th}^{1\text{GHz}} \rangle = 0.08 \pm 0.01$ . The average thermal fraction at 1.4 GHz in normal galaxies is  $\lesssim 10$  per cent (Kennicutt 1983b; Condon & Yin 1990).

The standard method applied here to derive the thermal fraction using the constant non-thermal spectral index is simplistic. Tabatabaei et al. (2007b) derived the thermal radio continuum in the galaxy M33 from the extinction corrected  $H_\alpha$  map instead of using a constant  $\alpha_{nt}$  across the galaxy. They find that the thermal fraction of M33 at 3.6 cm using the new method is  $23 \pm 14$  per cent lower than found by assuming a constant  $\alpha_{nt}$  across the galaxy. However, Tabatabaei et al. (2007b) note that the thermal fraction derived from the radio integrated spectrum of M33 using the standard method and the new method agree. Hence, assumption of a constant non-thermal spectral index to derive the thermal fraction is reasonable when the integrated spectrum is used.

Considering the small value of the thermal fraction in the total emission of NGC 2997 at low frequencies, we assume that the spectral power given in Table 5 is mostly non-thermal. We estimate the supernova rate ( $\text{yr}^{-1}$ ) in NGC 2997 from the non-thermal luminosity (Condon & Yin 1990). The estimated supernova rate for the disc and nuclear region is about  $\sim 0.08$  and  $\sim 0.01 \text{ yr}^{-1}$  respectively. In order to compare the SN rate per  $\text{kpc}^2$ , we assumed a diameter  $\sim 1.3$  and  $\sim 24.5 \text{ kpc}$  for the nucleus and the disc respectively. The SN rate per  $\text{kpc}^2$  for the nucleus and the whole disc is about  $\sim 8 \times 10^{-3} \text{ yr}^{-1} \text{ kpc}^{-2}$  and  $\sim 0.14 \times 10^{-3} \text{ yr}^{-1} \text{ kpc}^{-2}$  respectively. If we assume a filling factor of  $\sim 0.7$  for the disc, the SN rate for the disc is about  $\sim 0.2 \times 10^{-3} \text{ yr}^{-1} \text{ kpc}^{-2}$  i.e. the nuclear region has a SN rate which is 40 times higher than the rate in the disc.

The tight correlation between the radio continuum intensities and the FIR luminosities is known to be linear over a wide range in star formation rate from normal spirals to the most intense starbursts (Lacki et al. 2010). Roy et al. (1998) found that Seyfert galaxies with radio quiet cores follow the linear radio-FIR correlation similar to normal galaxies. NGC 2997 is a late type spiral galaxy and having no obvious companion (Milliard & Marcelin 1981). With the resultant steep spectral index  $\alpha = -0.92 \pm 0.04$  of NGC 2997, absence of an active nucleus (see section 4.3), and the observed logarithmic measure of FIR/radio flux density ratio at our observing frequencies, the linear correlation between FIR and radio emission exists in NGC 2997. For estimating various parameters like average formation rate of stars more massive than  $5 M_\odot$  ( $\text{SFR}(M \gtrsim 5 M_\odot) M_\odot \text{ yr}^{-1}$ ) and the ionization rate of the Lyman continuum photons ( $s^{-1}$ ) given in Table 7, we assumed a simple model with only one free parameter – the average formation rate of stars more massive than  $5 M_\odot$  (Condon 1992).

Radio counts of young Galactic SNRs suggest a radio supernova rate of  $0.013 \text{ yr}^{-1}$  (Caswell & Lerche 1979) or Type II supernova rate  $\nu_{SN} \sim 0.023 \text{ yr}^{-1}$  estimated by Tammann (1982). Our data suggest that the supernova rate in NGC 2997 is a factor of three to four times higher than that of our Galaxy. The Lyman continuum photon rate of the Galaxy is  $2 \times 10^{53} \text{ photons s}^{-1}$  (Güsten & Mezger 1982). The derived star formation rate in NGC 2997 suggest that the galaxy is a normal galaxy with intermediate star formation. The derived values of star formation rate and the Lyman continuum photon rate of NGC 2997 are less than the values derived for M82 by Condon (1992) but higher than our Galaxy. For M82, the star formation rate  $\text{SFR}(M \gtrsim 5 M_\odot)$  is  $\sim 2.2 M_\odot \text{ yr}^{-1}$ ,

**Table 6.** Total flux density measurements of NGC 2997

Frequency GHz	Flux density Jy	Reference
8.460	$0.034 \pm 0.004$	Han et al. (1999) <sup>a</sup>
5.010	$0.092 \pm 0.010$	Whiteoak (1970)
4.860	$0.067 \pm 0.011$	Han et al. (1999) <sup>a</sup>
4.850	$0.141 \pm 0.014$	Wright et al. (1996)
2.373	$0.160 \pm 0.010$	Han et al. (1999)
1.543	$0.255 \pm 0.020$	Han et al. (1999)
1.490	0.290	Condon (1987)
1.400	$0.235 \pm 0.010$	Condon et al. (1998)
1.272	$0.367 \pm 0.008$	This paper
0.616	$0.730 \pm 0.022$	This paper
0.332	$1.134 \pm 0.111$	This paper

a. Lower limits, because of missing spacing problems, not included in fit in Fig.3

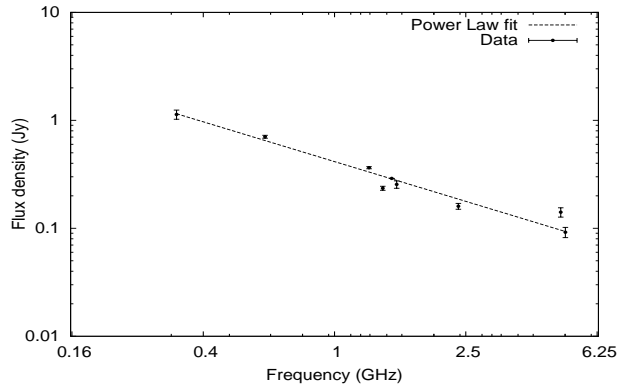


**Figure 3.** The total emission spectra of NGC 2997. In addition to our three GMRT data points, the data given in Table 6 are also plotted. The dashed line is the best least-squares fitting to the data with a power law index  $\alpha = -0.92 \pm 0.04$

the ionization rate is  $N_{uv} \sim 8 \times 10^{53} \text{ s}^{-1}$  and the radio supernova rate is  $\nu_{SN} \sim 0.1 \text{ yr}^{-1}$  (Condon 1992).

## 4.2 Spectral index (SI) distribution

The spectral index ( $S_\nu \propto \nu^\alpha$ ) distribution across the galaxy was determined by using total intensity maps of identical beamsize at 1272 and 332 MHz respectively. Both the maps were convolved with a circular Gaussian beam of 18 arcsec in size and all points below  $3\sigma$  level were blanked out. Spectral index map ( $\alpha_{1.27,0.33}$ ) was then derived using the COMB task in AIPS. The SI map between 1272 and 332 MHz is shown as a grey scale image in Fig.4 (left) with the 1272 MHz radio contour map superimposed on it. The uncertainty for the measured SI map is shown in the right panel of Fig.4. The spectral index measured over most of the disc shows uncertainty in the range of 0.05 to 0.25. The uncertainty map (Fig.4 right) shows intense regions (i.e. high S/N) having error  $\lesssim 0.15$  whereas uncertainty increases in the fainter parts of the galaxy. Strong features registered with position errors of the order of 3 to 4

**Table 7.** Estimated parameters for NGC 2997

	Disc	Nuclear region
1. Star-formation rate ( $M_\odot \text{ yr}^{-1}$ )	1.9	0.2
2. The ionization rate ( $10^{53} \text{ s}^{-1}$ )	6.7	0.8
3. The supernova rate ( $\text{yr}^{-1}$ )	0.08	0.01

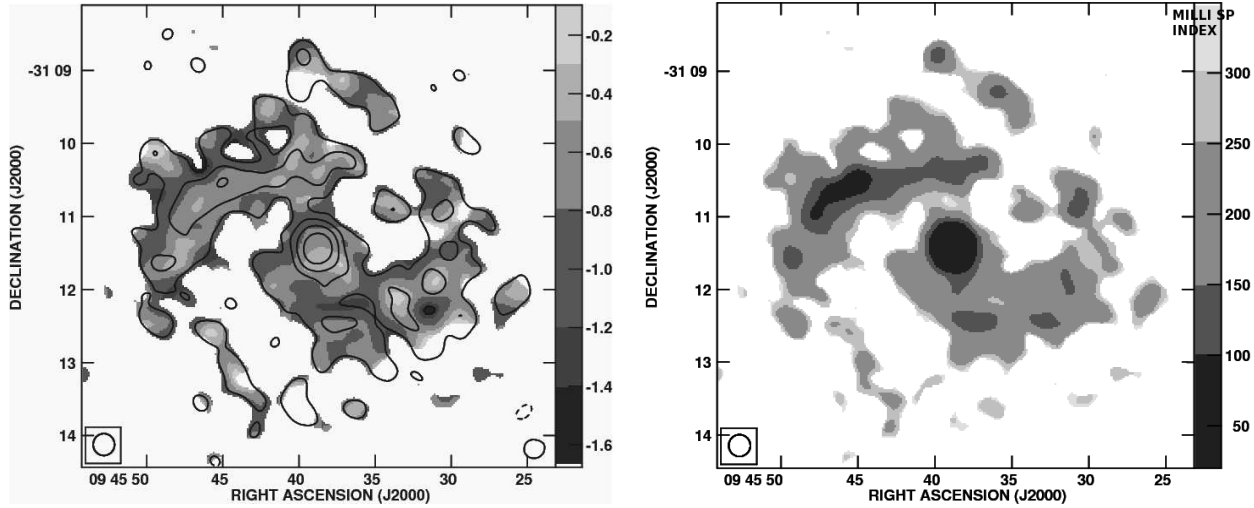


**Figure 4.** Left panel shows grey-scale spectral index image ( $\alpha_{1.27,0.33}$ ) between 1272 and 332 MHz and right panel shows the image of spectral index uncertainty. The radio contour map at 1272 MHz superimposed on the grey-scale spectral index image with contours  $(-3, 3, 6, 12, 24) \times \sigma$  level. The rms  $\sigma$  is 0.5 mJy per beam area and the nucleus is the brightest region of the galaxy. All images in this figure are restored with a beamsize of 18 arcsec, the beamsize is indicated at the BLC.

arcsec in total intensity maps can make larger changes in the spectral index measurements. The errors in RA and DEC in our total intensity maps are  $\sim \pm 0.22^\circ$  and  $\sim \pm 2$  arcsec, respectively.

The SI map in Fig. 4 shows that the radio spectrum is flatter in nature wherever brightness peaks such as intense spiral arms and nucleus exist, whereas radio spectrum of the outer parts of spiral arms show steeper spectrum. The radio emission from normal galaxies is known to be closely related to the population of young massive main sequence stars which ionizes the HII regions causing the free free thermal radio emission. The supernova explosions of these young massive stars accelerate the relativistic electrons causing the non-thermal synchrotron emission. As the spectral indices of Galactic supernovae remnants (SNRs) are known to show a broad range ( $-0.2 < \alpha < -0.8$ ) with a mean value of  $\sim -0.5$  (Trushkin 1999) and considering that the thermal fraction of the observed total flux densities at low frequencies is less than 10 per cent, the relative flatter spectral index regions in spiral arms could suggest direct contribution of non-thermal emission by SNRs. The spectral index value which increases up to  $\sim -1.2 \pm 0.2$  in the outer parts of the spiral arms indicates the energy losses of the relativistic electrons while they diffuse away out of their place of origin in star forming regions.

We measured a spectral index  $-0.6 \pm 0.04$  for the nucleus by a single power law fit to the flux densities listed in Table 4 (source 1). This is consistent with the mean spectral index value of the nucleus in the SI map shown in Fig.4 ( $\alpha_{1.27,0.33} \sim -0.62 \pm 0.1$ ). A relatively flatter spectral index of the nuclear region might be due to a younger population of particles, due to the thermal contribution by ionized gas in massive-star clusters and SNR.

The spatial spectral index for the ridge-component in the northern spiral arm varies from  $-0.78 \lesssim \alpha_{1.27,0.33} \lesssim -0.46$ . The source 3 in the ridge-component (Fig.4, left) is a giant HII region and the core source in this region is classified as a thermal source (Firpo et al. 2005). The spectral index value for source 3 is  $\sim -0.06$  (see Table 4) and confirms the thermal nature of emission.

### 4.3 The circumnuclear ring

We detect a strong nuclear source in NGC 2997 at all the wavebands which is resolved into a circumnuclear starforming ring in our high resolution 1272 MHz image. NGC 2997 is an intermediate type SAB(rs)c galaxy with several hotspots. The circumnuclear star forming ring has been observed in the optical and NIR (Maoz et al. 1996; Elmegreen et al. 1999). Circumnuclear rings are observed in 20 per cent of all spiral galaxies and mostly occur in barred galaxies (Knapen 2005). Observational studies (Allard et al. 2005; Böker et al. 2008) show that the circumnuclear ring can arise due to the bar driven radial inflow of magnetized gas materials which gets accumulated in a ring near the location of inner Lindblad resonances. There are two models which explain the star formation in circumnuclear rings : (i) in the gravitational instability or “popcorn” (Elmegreen 1994; Böker et al. 2008) model, star formation is driven by stochastic gravitational fragmentation along the ring where the star forming regions have a regularly spaced distribution (Elmegreen et al. 1999). (ii) in the “pearls on a string” model, the gas along the bar that flows into the ring is compressed near the contact points. Star formation is then triggered in these over density contact regions. Observationally an age gradient in the star forming regions is seen along either half of the ring (Allard et al. 2005; Böker et al. 2008).

We made a high resolution image at 1.27 GHz using robust weighting of  $-5$  in the task IMAGR. The resulting angular resolution of 3 arcsec ( $\sim 200$  pc) resolved the circumnuclear ring (see Fig.5) into five star-forming clumps i.e. hotspots. We measured the position, peak intensity and integrated flux-density of each hotspot by fitting a Gaussian using the task JMFIT in AIPS. The position for each component is listed using seconds of RA and arcsec of DEC in Table 8. The observed luminosity for the individual hotspot is between 0.16 to  $1.58 \times 10^{20} \text{ W Hz}^{-1}$  at 20 cm band with a 200 pc resolution. We also calibrated and imaged VLA archival data of this galaxy at 4.8 GHz. The resulting image shown as grey scale in Fig.5 (left) also detects the circumnuclear ring coincident with the 1.27 GHz ring. Fig.5 (right) shows the 1.27 GHz radio contour map overlaid on *HST V* band gray-scale image (Maoz et al.

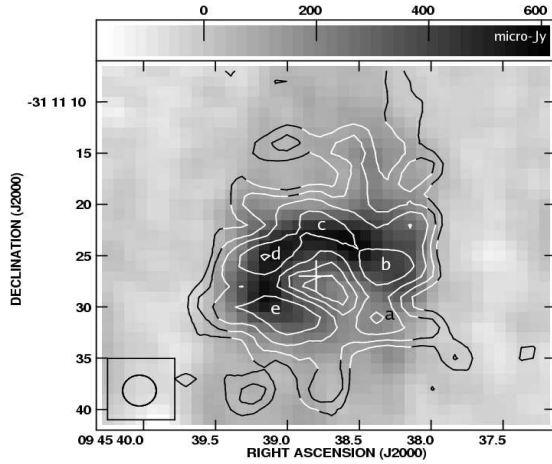


**Fig.5 left:** Contour levels are at 0.24, 0.4, 0.56, 0.72, 0.88, 1.04, 1.2, 1.36 mJy beam<sup>-1</sup>, the peak brightness is 1.39 mJy beam<sup>-1</sup>

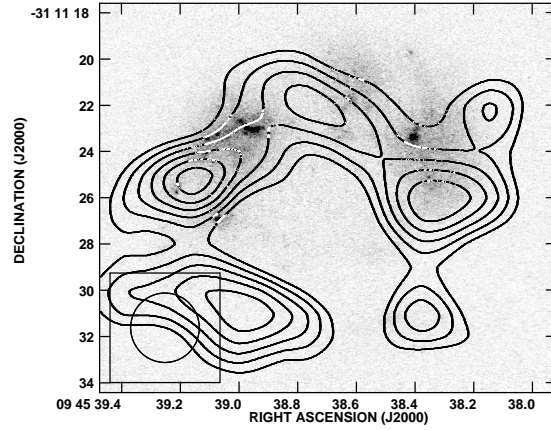


**Fig.5 right:** Contour levels are at 0.72, 0.84, 0.96, 1.07, 1.2, 1.32 mJy beam<sup>-1</sup>, the peak brightness is 1.39 mJy beam<sup>-1</sup>

**Figure 5.** The GMRT radio contour map of the nuclear region at 1.27 GHz with an angular resolution of  $3 \times 3$  arcsec<sup>2</sup> overlaid on (left) gray-scale archival VLA 4.8 GHz C band image (restored with a beamsize  $3 \times 3$  arcsec<sup>2</sup>, PA= 0°) and (right) gray-scale HST archival V band 2300Å image (Courtesy, Maoz et al. (1996); resolution  $\sim 0.05$  arcsec, PA= 84.30°).

**Table 8.** Radio hotspots in the circumnuclear region of NGC 2997

Hotspot	Position (J2000) RA (sec), DEC (arcsec)	Deconvolved angular size (arcsec <sup>2</sup> PA)	Peak Intensity (mJy beam <sup>-1</sup> )	Integrated flux density (mJy)	Radio luminosity (10 <sup>20</sup> W Hz <sup>-1</sup> )
a	38.37,31.01	1.7 × 1.3 @167°	0.61	0.77 ± 0.17	0.16
b	38.32,25.77	7.5 × 5.0 @ 88°	1.34	7.0 ± 0.5	1.52
c	38.78,22.31	12.5 × 4.0 @ 76°	0.77	5.0 ± 0.6	1.17
d	39.12,25.00	7.7 × 2.1 @122°	0.96	3.27 ± 0.3	0.7
e	39.02,30.86	9.4 × 4.0 @71°	1.34	7.36 ± 0.5	1.58

1996). The radio ring is coincident but more extensive than the observed structure of the ring in the V band. This is likely to be due to the lower angular resolution at radio wavelengths and partly probably due to extinction at optical wavelengths which Elmegreen et al. (1999) estimate to be about 3 magnitudes in the vicinity of the ring. The morphological structure of the circumnuclear region in our 1.27 GHz radio contour map is similar to the contour maps of relative intensities in U band published by Meaburn & Terrett (1982) using the SAAO 1.9-m reflector.

Our radio contour map and the gray-scale images in the UV (2300 Å) and radio (4.8 GHz) band shown in Fig.5 indicate that there is no detectable radio continuum emission from the central part of the nucleus, confirming that there is no radio-loud AGN in the center of this galaxy. Maoz et al. (1996) observed circumnuclear rings in five barred or weakly barred spiral galaxies of type Sc (including NGC 2997) and none of the rings hosted an AGN at its centre. The quiescent phase of the nucleus was also noted in the detailed study of the NGC 2997 nucleus by Walsh et al. (1986). A large number of hotspots are observed on a complete circumnuclear ring of NGC 2997 at NIR (Elmegreen et al. 1999) whereas only three northern star-forming regions are visible in the V band image. We note that the intense NIR hotspots located in the northern part of the ring correlate with the radio hotspots. Weak radio emission is detected from the southern parts of the ring although hotspots are not distinguishable. The faint emission along the southern half of the ring is seen in UV (Maoz et al. 1996), U (Meaburn & Terrett 1982) band image. Faint southern hotspots are also seen in NIR ring which Elmegreen et al. (1999) attribute to the heavy dust ex-

tingtion since the southern hotspots are being observed through the dust lanes. A slight offset between the optical and radio positions of the hotspots are observed. This could be attributed to the poor angular resolution of the radio data ( $\sim 3$  arcsec) as compared to the excellent resolution of the optical data ( $\sim 0.05$  arcsec) and dust extinction near the star forming peaks.

The circumnuclear ring that we detect in radio has a deconvolved diameter of  $11.6 \pm 0.08$  arcsec i.e.  $\sim 750$  pc. The separation between the hotspots ranges from  $\sim 190$  to 370 pc. This is comparable to the NIR where the diameter of the ring is  $\sim 570$  pc ( $\sim 8.7$  arcsec) and the spacings between hotspots is  $\sim 200$  pc (Elmegreen et al. 1999). This is typical of the circumnuclear rings detected in other galaxies. The average size of the nucleus from the photometric and morphological analysis of the galaxies with peculiar nuclei is quoted to be less than 800 pc (Pastoriza 1975).

We compared the circumnuclear ring (CNR) in NGC 2997 to the well studied CNR in NGC 1097 (Walsh et al. 1986; Barth et al. 1995; Beck et al. 1999; Sandstrom et al. 2010). The CNR of NGC 1097 has  $\sim 1.5$  kpc diameter (Beck et al. 2005) and a LINER/Seyfert 1 AGN at its centre. Three prominent radio hotspots are seen at 3.5 cm in NGC 1097 (Beck et al. 2005) whereas four bright and one faint hotspots are observed in NGC 2997 at 20 cm (see Fig.5). No azimuthal age gradient is seen in massive stars of both the rings with ages less than  $10^7$  to  $10^8$  yrs (Maoz et al. 1996; Elmegreen et al. 1999; Sandstrom et al. 2010) and both rings show regular distribution of hotspots (Barth et al. 1995; Elmegreen et al. 1999; Beck et al. 2005) which lends support to the gravitational instability model (Elmegreen 1994) for the star formation in the



CNR. The CNR in NGC 1097 is formed due to the gas driven by bar potential. Various observational studies show that NGC 2997 does not possess either a prominent large scale bar or an active nucleus (Walsh et al. 1986; Maoz et al. 1996), hence unlike NGC 1097 gas accumulation in the CNR of NGC 2997 is unclear. However, Fast Magnetohydrodynamic Density Waves (FMDWs) at the modified inner Lindblad resonance (mILR) model (Lou et al. 2002; Lou 2003) can explain the formation of CNR in NGC 2997.

We estimate an equipartition field in the central nuclear region of diameter  $\sim 750$  pc to be about  $30 \mu\text{G}$ . This is similar to the field strength of  $34 \mu\text{G}$  estimated by Han et al. (1999) for the central region of NGC 2997 and  $40 \mu\text{G}$  estimated for the CNR in NGC 1097 by Beck et al. (1999). The equipartition field for the radio hotspots in NGC 2997 ranges from  $\sim 30$  to  $50 \mu\text{G}$ . We estimate a disc field of  $\sim 4 \mu\text{G}$  for NGC 2997.

We compared the luminosity of radio hotspots in circumnuclear region of NGC 2997 with the circumnuclear radio hotspots in other galaxies such as NGC 253, 1365 and 1808. NGC 253 is a nearby ( $d \sim 2.5$  Mpc) starburst galaxy, in which Ulvestad (2000) detected 22 compact circumnuclear sources at 20 cm with  $\sim 28$  pc resolution. The detected circumnuclear sources of NGC 253 have typical radio power of  $2 \times 10^{18} \text{ W Hz}^{-1}$ . Stevens et al. (1999) detected seven hotspots in the circumnuclear region of NGC 1365 at 3 and 6 cm with a 100 pc resolution ( $d \sim 20$  Mpc). The luminosity of circumnuclear hotspots for NGC 1365 at 20 cm (derived using a SI from 6 and 3 cm) ranges from  $\sim 0.8$  to  $2 \times 10^{20} \text{ W Hz}^{-1}$ . Similarly, Collison et al. (1994) detected hotspots in NGC 1808 with a resolution of 98 pc. The luminosity of circumnuclear hotspots in NGC 1808 ( $d \sim 9.9$  Mpc) at 20 cm (derived using a SI between 6 and 3.6 cm) ranges from  $\sim 0.2$  to  $3.8 \times 10^{20} \text{ W Hz}^{-1}$ . Thus, the average luminosity of hotspots in a CNR observed with  $\sim 100$  pc resolution appears to be  $10^{19}$  to a few times  $10^{20} \text{ W Hz}^{-1}$  at 20 cm. It is likely that the hotspots are composed of several  $2 \times 10^{18} \text{ W Hz}^{-1}$  clumps as seen in NGC 253 in addition to diffuse non-thermal emission. Assuming that the observed emission at 1.27 GHz from the circumnuclear hotspots is mostly non-thermal in nature, we derived the SN rate based on Condon & Yin (1990) equation. The median SN rate value for the discrete components in NGC 2997 ring is  $\sim 0.001 \text{ yr}^{-1}$ . The median value of average formation rate of stars ( $\text{SFR}(M \gtrsim 5M_{\odot}) M_{\odot} \text{ yr}^{-1}$ ) estimated for the hotspots is  $\sim 0.024 M_{\odot} \text{ yr}^{-1}$ .

The spectral index  $\alpha_{4.8,1.27}$  of the CNR in NGC 2997 is  $\sim -0.64 \pm 0.1$ . We could not estimate the spectral index of the individual hotspots since these were not clearly discernible in the convolved 4.8 GHz map (see Fig.5). NGC 6951, unlike NGC 2997, hosts a central AGN and has a marginally larger diameter ( $\sim 1$  kpc) of the CNR but both the rings show hotspots which form an almost complete ring. In NGC 2997, the radio ring is fainter to the south whereas in NGC 6951 the ring appears to be broken in the north and south (Saikia et al. 2002). The spectral index of the circumnuclear emission in NGC 6951 between 20 and 6 cm was found to be  $-0.84$  (Ho & Ulvestad 2001). The radio spectrum of the hotspots in the CNR of other galaxies exhibit a large range in spectral index. For example, the CNR in NGC 613 has a spectral index of  $-0.65$  between 2 and 6 cm (Hummel & Jörsäter 1992) similar to NGC 2997, whereas the spectral index of the individual compact sources (total 19) in the CNR of NGC 4736 exhibit spectral index ranging from 0.1 to  $-0.8$  between 6 and 20 cm (Duric & Dittmar 1988). Similar kind of distribution is also noted in the CNR of NGC 1365 between 3 and 6 cm by Stevens et al. (1999). Out of seven hotspots detected in the ring of NGC 1365, four hotspots show steep spectrum and rest show flat spectrum with the spectral index ranging

from 0.04 to  $-0.4$  (Stevens et al. 1999). Stevens et al. (1999) attribute synchrotron emission from hotspots to electrons accelerated by SN and SNRs. The spectral indices of circumnuclear hotspots detected between 3.6 and 6 cm in NGC 1808 (Collison et al. 1994) are also consistent with them being dominated by SNRs. Utilizing a V band *HST* exposure of NGC 2997, Maoz et al. (1996) determined the numerous compact (few pc radius) sources distributed along the ring that are probably young (less than  $10^8$  yr) and massive ( $\sim 10^5 M_{\odot}$ ) clusters of stars that are gravitationally bound.

## 5 SUMMARY

We have presented high resolution radio continuum maps of NGC 2997 at 332, 616 and 1272 MHz. To the best of our knowledge these are the first images of the galaxy at  $\nu < 1.4$  GHz. The radio continuum features detected in our observation bands are described, in detail, along with the spectral index values. The best-fitting single power law model to the integrated radio spectrum of NGC 2997 gives a spectral index  $\alpha = -0.92 \pm 0.04$ . The best-fitting value of  $\alpha = -0.79 \pm 0.07$  obtained using only the low-frequency GMRT data suggests a break in the spectrum at  $\nu < 1$  GHz. We put an upper limit of 10 per cent on the thermal fraction at 1 GHz.

The spectral power of NGC 2997 at our observing frequencies is in the range of  $7.9$  to  $24.4 \times 10^{21} \text{ W Hz}^{-1}$ . The derived logarithmic measure of FIR/radio flux density ratio,  $\hat{q}_{\text{FIR}}$  parameter is  $\sim 2.19 \pm 0.03$ , which is near the median for spiral galaxies at 1.4 GHz,  $\hat{q}_{\text{FIR}} \approx 2.30$  (Condon 1992). The estimated values for average star formation rate  $\text{SFR}(M \gtrsim 5M_{\odot})$  is  $1.9 M_{\odot} \text{ yr}^{-1}$ , the supernovae rate is  $0.08 \text{ yr}^{-1}$ , and the production rate of the Lyman continuum photons is  $6.7 \times 10^{53} \text{ s}^{-1}$ . The resultant logarithmic measure of FIR/radio flux density ratio and the intermediate average star formation rate confirms that NGC 2997 is a normal galaxy.

The low frequency spectral index distribution map ( $\alpha_{1.27,0.33}$ ) of NGC 2997 shows that the radio spectrum is flatter in nature near brightness peaks such as in intense spiral arm regions and nucleus, whereas radio emission from the low surface brightness regions shows a steeper spectrum. The measured spectral index for the nucleus between 332 and 1272 MHz is  $\alpha \sim -0.6 \pm 0.04$ .

The radio continuum map at 1272 MHz with an angular resolution of 3 arcsec ( $\sim 200$  pc) reveals a circumnuclear ring structure with five radio hotspots. No radio continuum emission at the centre of the galaxy is detected indicating that there is no radio-loud AGN. Part of the ring to the south is faint. The circumnuclear ring is similar to that observed at other wavebands from the galaxy and in other galaxies. It has a deconvolved diameter of  $\sim 750$  pc and the separation between hotspots range from  $\sim 190$  to  $370$  pc. We estimate an equipartition field in the central nuclear region of diameter  $\sim 750$  pc to be about  $30 \mu\text{G}$ . The observed luminosity for the individual hotspot is about  $10^{20} \text{ W Hz}^{-1}$ . The median SN rate and average formation rate of stars  $\text{SFR}(M \gtrsim 5M_{\odot})$  for the hotspots in the ring are  $0.001 \text{ yr}^{-1}$  and  $0.024 M_{\odot} \text{ yr}^{-1}$  respectively.

## ACKNOWLEDGMENTS

We thank the staff of the GMRT who have made these observations possible. GMRT is run by the National Centre for Radio Astrophysics of the Tata Institute of Fundamental Research. We thank the anonymous referee for useful comments on the manuscript. J. Kodilkar thanks the Dean of the GMRT, Prof. Y. Gupta for his support. One of the authors (SA) wishes to thank R. Wielebinski for bringing to his notice the importance of low frequency observation of NGC 2997. This research has made use of the NASA/IPAC Extragalactic Database which is operated by the Jet Propulsion Laboratory, Caltech under contract with the NASA.

## REFERENCES

- Allard E.L., Peletier R.F. and Knapen J.H., 2005, *ApJ*, 633, L25
- Ananthakrishnan S., 2005, *Proc. 29th International Cosmic Ray conference*, Pune, 10, 125
- Barth A. J., Ho L. C., Filippenko A. V., and Sargent W. L., 1995, *AJ*, 110, 1009
- Beck R., Ehle M., Shoutenkov V., Shukurov A., and Sokoloff D., 1999, *Nature*, 397, 324
- Beck R., Ehle M., Fletcher A., Harnett J., Shoutenkov V., Shukurov A., and Sokoloff D., 2005, *AIP Conf. Proc.*, 783, 216
- Böker T., Falcón-Barroso J., Schinnerer E., Knapen, J. H., and Ryder S., 2008, *AJ*, 135, 479
- Caswell J.L. and Lerche I., 1979, *MNRAS*, 187, 201
- Collison P.M., Saikia D.J., Pedlar A., Axon D.J., and Unger S.W., 1994, *MNRAS*, 268, 203
- Condon J.J., 1987, *A&AS*, 65, 485
- Condon J.J., 1992, *A&AR*, 30, 575
- Condon J.J. and Broderick J.J., 1988, *AJ*, 96, 30
- Condon J.J. and Yin Q.F., 1990, *ApJ*, 357, 97
- Condon J.J., Cotton W. D., Greisen E. W., Yin Q. F., Perley R. A., Taylor G. B., and Broderick J. J., 1998, *AJ*, 115, 1693
- Condon J.J., Frayer D. T., Broderick J. J., 1991b, *AJ*, 101, 362
- de Vaucouleurs G., de Vaucouleurs A., Corwin JR. H. G., Buta R. J., Paturel G., and Fouque P., 1991, *Third Reference Catalogue of Bright Galaxies*. Springer, New York
- Duric N. and Dittmar M. R. 1988, *ApJ*, 332, L67
- Elmegreen, G. B., 1994, *ApJ*, 425, L73
- Elmegreen D.M., Chromey F.R., Sawyer J.E., and Reinfeld E.L., 1999, *AJ*, 118, 777
- Fathi K., Storch-Bergmann T., Riffel R.A., Wing C., Axon D.J., Robinson A., Capetti A., Marconi A., 2006, *ApJ*, 641, L25
- Firpo V., Bosch G., Morrell N., 2005, *MNRAS*, 356, 1357
- Fitt A.J., Howarth N.A., Alexander P. and Lasendby, 1996, *MNRAS*, 255, 146
- Garcia A. M., 1993, *VizieR Online Data Catalog*, 410, 47
- Grosbøl P., Dottori H., and Gredel R., 2006, *A&A*, 453, L25
- Güsten R. and Mezger P.G., 1982, *Vistas in Astronomy*, 26, 159
- Han J.L., Beck R., Ehle M., Hynes R.F., and Wielebinski R., 1999, *A&A*, 348, 405
- Helou G., Soifer B. T., Rowan-Robinson M., 1985, *ApJ*, 298, L7
- Ho, L. C. and Ulvestad, J. S., 2001, *ApJs*, 133, 77
- Hummel E., 1991, *A&A*, 251, 442
- Hummel E. and Jörsäter S., 1992, *A&A*, 261, 85
- Israel F.P. and Mahoney M.J., *ApJ*, 1990, 352, 30
- Knapen J.H., 2005, *A&A*, 429, 141
- Kennicutt R., 1983b, *A&A*, 120, 219
- Koribalski B. S., Staveley-Smith L., Kilborn V.A. et al., 2004, *AJ*, 128, 16
- Lacki B. C., Thompson T. A., Quataert E., 2010, *ApJ*, 717, 1
- Lou Y.Q., 2003, *ATCA Astronomica Sinica*, 44, 172
- Lou Y.Q., Walsh W.M., Han J.L., and Fan Z., 2002, *ApJ* 567, 289
- Maoz D., Barth A. J., Sternberg A., Filippenko A.V., Ho L. C., Macchetto F.D., Rix H.-W., Schneider D.P., 1996, *AJ*, 111, 2248
- Meaburn J. and Terrett D.L., 1982, *MNRAS*, 200, 1
- Men H. and Han J. L., 2005, *Chin. J. Astron. Astrophys.*, 5, 49
- Milliard B. and Marcelin M., 1981, *A&A* 95, 59
- Niklas S., Klein U. and Wielebinski R., 1997, *A&A* 322, 19
- Pastoriza M. G., 1975, *Ap&SS*, 33, 173P
- Peterson C. J., 1978, *ApJ*, 226, 75
- Pohl M., Schlickeiser R., and Hummel E., 1991, *A&A*, 250, 302
- Roy A.L., Norris R.P., Kesteven M.J., Troup E.R. and Reynolds J.E., 1998, *MNRAS*, 301, 1019
- Sandstrom K., Krause O., Linz H., Schinnerer E., Dumas G., Meidt S. et al., 2010 *A&A* 518, L59
- Saikia D.J., Phookun B., Pedlar A., and Kohno K., 2002, *A&A*, 383, 98
- Stevens I.R., Forbes D.A., and Norris R.P., 1999, *MNRAS*, 306, 479
- Swarup G., Ananthakrishnan S., Kapahi V.K., Rao A.P., Subrahmanya C.R., and Kulkarni V.K., 1991, *Current Science*, 60, 95
- Tabatabaei F.S., Beck R., Krügel, Krause M., Berkhuijsen E.M., Gordon K.D., and Menten K.M., 2007b, *A&A*, 475, 133
- Tammann G. A., 1982, In *Supernovae: A Survey of Current Research*, ed. Rees M.J., Stoneham R.J., 371
- Trushkin S. A., 1999, *Odessa Astronomical publications*, 12, 144
- Tully R.B., 1988, *Nearby Galaxies Catalog*, Cambridge University Press, Cambridge
- Ulvestad J.S., 2000, *AJ*, 120, 278
- Walsh J.R., Nandy K., Thompson G.I., Meaburn J., 1986, *MNRAS*, 220, 453
- Whiteoak J.B., 1970, *ApL*, 5, 29W
- Wright A. E., Griffith M. R., Hunt A. J., Troup E., Burke B. F., and Ekers R. D., 1996, *ApJS*, 103, 145W